

SCIENTIFIC REPORTS

OPEN

Precipitous change of the irreversible strain limit with heat-treatment temperature in Nb₃Sn wires made by the restacked-rod process

Najib Cheggour^{1,2,3}, Theodore C. Stauffer², William Starch³, Peter J. Lee³, Jolene D. Splett⁴, Loren F. Goodrich^{1,2} & Arup K. Ghosh⁵

The intrinsic irreversible strain limit $\varepsilon_{irr,0}$ of Nb₃Sn superconducting wires, made by the restacked-rod process and doped with either Ti or Ta, undergoes a precipitous change as a function of temperature θ of the final heat-treatment for forming the A15 phase. Nb₃Sn transitions from a highly brittle state where it cracks as soon as it is subjected to an axial tensile strain of any measurable amount, to a state more resilient to tensile strain as high as 0.4%. The remarkable abruptness of this transition (as most of it occurs over a range of only 10 °C) could pose real challenges for the heat-treatment of large magnets, such as those fabricated for the high-luminosity upgrade of the Large Hadron Collider (LHC). We named this behavior the *strain irreversibility cliff* (SIC) to caution magnet developers. The approach to fulfilling application requirements just in terms of the conductor's residual resistivity ratio *RRR* and critical-current density J_c is incomplete. Along with *RRR* and J_c wire specifications, and sub-element size requirements that reduce wire magnetization and instabilities effects, SIC imposes additional constraints on the choice of heat-treatment conditions to ensure mechanical integrity of the conductor.

After decades of extensive usage of the ductile Nb-Ti conductor in the fabrication of superconducting magnets for various particle-accelerator facilities, a significant leap will soon take place into a somewhat uncharted territory by introducing the brittle Nb₃Sn conductor in the high-luminosity upgrade of the large hadron collider (LHC) at the European organization for nuclear research (CERN)¹⁻³.

Previously, we reported that the high critical-current-density (J_c) Nb₃Sn wires made by the internal-tin rod-restacked process (RRP[®])⁴ exhibit a significantly higher intrinsic irreversible strain limit ($\varepsilon_{irr,0}$) when doped with Ti instead of Ta⁵— $\varepsilon_{irr,0}$ being the intrinsic axial strain that denotes the onset of irreversible degradation of transport critical-current I_c due to strain application. We also showed that Ti-doped wires withstand the effects of (at least) limited strain cycling well because of their high $\varepsilon_{irr,0}$ ⁵. These results prompted the use of Ti for doping RRP wires, though the reasons for these differences between Ti and Ta doping remained elusive⁶. Simultaneously, a tubular-type internal-tin Nb₃Sn wire, even doped with Ta, showed very strong values of $\varepsilon_{irr,0}$ (as high as 0.45%)⁷, thus indicating that Ta doping is not irremediably detrimental to strain properties of all Nb₃Sn wires, and that other parameters must be influential in determining the wire's resilience to strain.

All RRP samples investigated in the previous work were given a heat treatment (HT), for reacting Nb₃Sn, that followed a three-stage scheme typically used for these wires, with temperature θ at the final stage set at 640 °C for a dwell time of 48 hours. The other HT two pre-stages were 210 °C for 72 hours and 400 °C for 48 hours. Setting θ at, or slightly higher than, 640 °C by the high-luminosity research and development program, especially for the

¹Department of Physics, University of Colorado, Boulder, CO, 80309, USA. ²Quantum Electromagnetics Division, National Institute of Standards and Technology, Boulder, CO, 80305, USA. ³Applied Superconductivity Center, National High Magnetic Field Laboratory, Florida State University, Tallahassee, FL, 32310, USA. ⁴Statistical Engineering Division, National Institute of Standards and Technology, Boulder, CO, 80305, USA. ⁵Brookhaven National Laboratory, Upton, NY, 11973, USA. Correspondence and requests for materials should be addressed to N.C. (email: ncheggour@asc.magnet.fsu.edu)

Received: 8 May 2018

Accepted: 1 August 2018

Published online: 29 August 2018

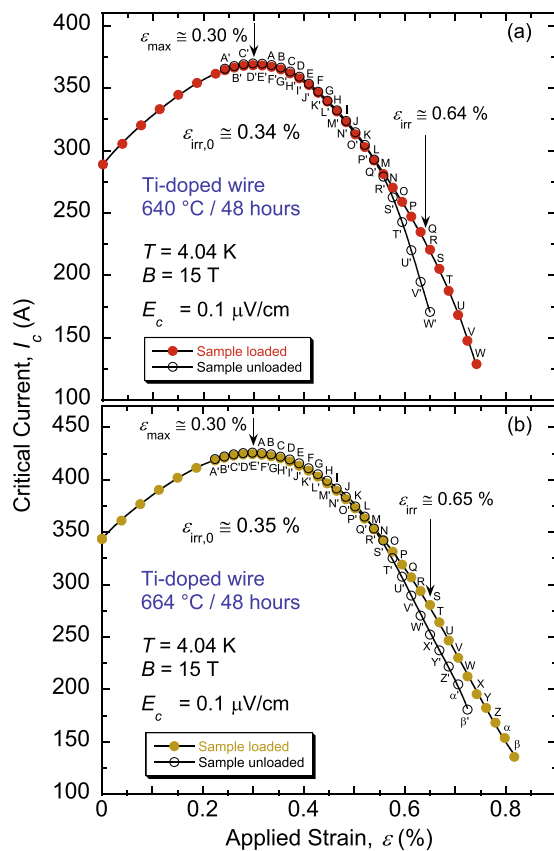


Figure 1. Comparison of $I_c(\varepsilon)$ at 4.04 K and 15 T for samples of an RRP Ti-doped Nb_3Sn wire (billet 11976-1), heat-treated for 48 hours at (a) 640 °C and (b) 664 °C. Beyond the reversible regime ($\varepsilon > \varepsilon_{irr}$), the unloaded curve deviates more from the loaded curve for the 640 °C heat-treatment, indicating a more pronounced irreversible degradation of I_c . The sample was loaded and partially unloaded (by constant axial-strain steps of about 0.09%) to obtain the “loaded” and “unloaded” $I_c(\varepsilon)$ curves, represented by solid and empty symbols, respectively. Corresponding loaded and unloaded points are labelled by unprimed and primed letters, respectively (for example, strain point A' is obtained after partially unloading axial strain off the sample from the strain point A). ε_{irr} is defined as the applied strain that produces the first splitting of these two curves. ε_{max} is the applied strain that compensates for the sample's pre-compressive strain, which arises from cooling the sample from heat-treatment temperature to 4 K and the thermal-contraction mismatch amongst the wire constituents as well as Cu-Be material of the Walters' spring (the sample was soldered to the spring). $\varepsilon_{irr,0}$ ($=\varepsilon_{irr} - \varepsilon_{max}$) is the intrinsic irreversible strain limit.

earlier RRP wires that had a standard ratio Nb/Sn = 3.4, was so that the residual resistivity ratio (RRR) of the wires remained sufficiently high (≥ 150 in undeformed strands, ≥ 100 in cabled strands) to insure a good electrical and thermal stability during operations of magnets made of these conductors^{8–10}. This HT schedule in fact does not maximize J_c and, as such, J_c potential is traded off for a better value of RRR⁸.

Results

Critical-current degradation beyond the irreversible strain limit. First, we compared samples of a Ti-doped billet reacted at 640 and 664 °C to verify that increasing θ slightly to gain higher J_c does not affect $\varepsilon_{irr,0}$. We investigated RRP billet 11976-1, of the design 108/127 [i.e., 108 Nb_3Sn sub-elements distributed around 19 Cu sub-elements located at the billet center, making it 127 restacked rods in total], and diameter of 0.82 mm. Effectively, these two HTs yielded very similar values of $\varepsilon_{irr,0}$ (see Fig. 1; additional details of how measurements are carried out and $\varepsilon_{irr,0}$ is determined can be found in^{11,12}). Simultaneously, we noticed a difference in the amount of I_c degradation in the irreversible strain regime (intrinsic strain $> \varepsilon_{irr,0}$) such that the unloaded curve deviates more from the loaded curve for 640 °C, as evidenced in Fig. 1(a,b). Indeed, the relative degradation of I_c between the loaded and unloaded points that have the same applied axial strain ε (for example strain points R and W' in Fig. 1(a)) is clearly different for the two HTs. This is detailed further in Fig. 2, where data are shown for two samples per HT, three pairs of voltage taps per sample, each probing a sample segment of about 8 cm in length corresponding to one full turn of the sample soldered onto a Cu-Be Walters spring^{13–15}. This I_c relative degradation has a small progression initially for strain just above $\varepsilon_{irr,0}$ (located at the flat-region end in Fig. 2), then becomes precipitous as strain is increased further. The rate of the precipitous degradation is approximately three times larger for the samples reacted at 640 °C in comparison to 664 °C, for the specific protocol used in these measurements

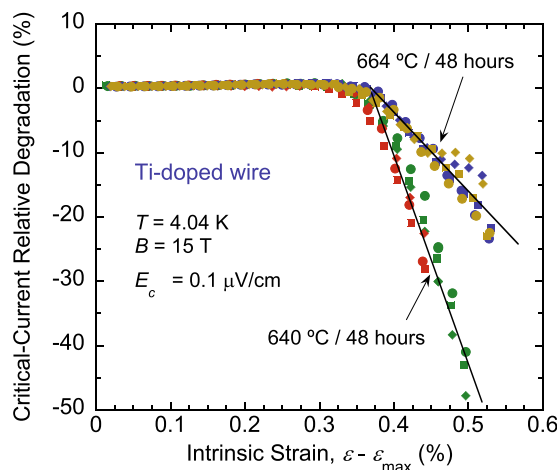


Figure 2. Critical-current relative degradation, defined as the I_c drop for an unloaded strain point relative to the loaded strain point at the same applied strain [for example points W⁷ and R in Fig. 1(a)]. Data were obtained at 4.04 K and 15 T for samples of an RRP Ti-doped Nb₃Sn wire (billet 11976-1), heat-treated for 48 hours at 640 °C and 664 °C. The rate of I_c degradation beyond $\varepsilon_{irr,0}$ ($=\varepsilon_{irr} - \varepsilon_{max}$) is about three times larger for 640 °C, for the specific protocol used in these measurements (described in Fig. 1 caption). Results are shown for two samples per heat-treatment temperature; for three segments (≈ 8 cm long each) per sample. Same color was used for symbols depicting data of a given sample, and each symbol of a given color represents one sample segment.

(described in Fig. 1 caption). Hence, even though irreversible effects (due presumably to cracking of Nb₃Sn) initiate at similar strains ($\varepsilon_{irr,0} \approx 0.35\%$), resilience of these samples to more cracking and to crack propagation is most probably different, even for such a small change in θ between the two HTs. Certainly, magnets must be designed so that strain on Nb₃Sn filaments never exceeds $\varepsilon_{irr,0}$, but analysis of the irreversible data appears informative.

Heat-treatment temperature effects; discovery of the strain irreversibility cliff. This finding opened the prospect that the fracture toughness of Nb₃Sn could be manipulated through heat-treatment optimization, and prompted us to investigate the effects of HT schedule in more detail. We studied Ti and Ta-doped billets, RRP 11976-1 and 13711-2, respectively, both having a standard Sn content (ratio Nb/Sn = 3.4), the same wire design (108/127), diameter (0.82 mm), and filaments twist pitch (13 mm). The non-Cu areas were 48.9% and 46.5% of the wires cross-sections, respectively. The nominal doping amounts were 1.5 and 4 at. % of Ti and Ta, respectively. We varied θ widely from 610 to 752 °C to study $\varepsilon_{irr,0}$ and irreversible effects, regardless of the RRR constraints. The dwell time at θ was kept at 48 hours and the two HT pre-stages were unchanged to make data comparisons more straightforward. Strain measurements were made on no less than 50 samples in total, and data taken on three segments (each ≈ 8 cm long) per sample. Samples were immersed in liquid helium at a temperature of 4.04 to 4.07 K, and were subjected to an applied magnetic field of 15 T. We used a Cu-Be Walters spring to strain samples *in-situ*^{13–15}. Determinations of I_c values presented herein were made at the electric-field criterion E_c of 0.1 $\mu\text{V}/\text{cm}$. Expanded uncertainties ($k=2$) due to random effects in estimating θ , I_c , and $\varepsilon_{irr,0}$ were 3 °C, 2% and 0.03% strain, respectively. The uncertainties for I_c and $\varepsilon_{irr,0}$ are based on type A evaluations of uncertainty, while the uncertainty for θ is based on type B evaluation of uncertainty¹⁶.

Whereas this study was prompted by the effect described above of $I_c(\varepsilon)$ in the irreversible strain regime (Figs. 1 and 2), it turned out that $\varepsilon_{irr,0}$ itself is strongly affected by θ . Examples of this dependence of $\varepsilon_{irr,0}$ on θ are depicted in Fig. 3 that show the underlying $I_c(\varepsilon)$ data of Ta-doped Nb₃Sn samples heat-treated at 642 °C and 678 °C (Figs. 3(a,b), respectively). $\varepsilon_{irr,0}$ improved significantly from 0.08% to 0.31% for the sample reacted at the higher θ . The complete behavior of $\varepsilon_{irr,0}$ as a function of θ is shown in Fig. 4(a), where each data point represents an average value of $\varepsilon_{irr,0}$ over six to nine segments (i.e., two to three samples per HT). The data reveal an abrupt and large change in $\varepsilon_{irr,0}$ with θ for both the Ti- and Ta-doped conductors. Surprisingly, Ta-doped wire can exhibit high $\varepsilon_{irr,0}$ for $\theta > 650$ °C, and Ti-doped wire can show significantly reduced $\varepsilon_{irr,0}$ for $\theta < 640$ °C, contrasting with conclusions in ref.⁵ according to which $\varepsilon_{irr,0}$ of Ta-doped RRP wires is inherently close to zero and that of Ti-doped wires is intrinsically high. Essentially, these Nb₃Sn wires go through a transition from a highly brittle state to a strain-resilient state. What is also remarkable, and potentially problematic for heat-treating magnets, is the very narrow range of θ over which this transition takes place. This range is 25 to 29 °C overall, but the bulk of the transition (i.e., $0.07\% \leq \varepsilon_{irr,0} \leq 0.3\%$) occurs over only 10 °C (Fig. 4(a)). Moreover, it is located around the domain of temperatures typically used for heat-treating RRP wires. We named this behavior the *strain irreversibility cliff* (SIC). For the Ti-doped wire, SIC is shifted to lower temperatures by about 10 to 12 °C as compared to that of the Ta-doped wire.

These results clearly demonstrate that the doping element is not a major factor in determining $\varepsilon_{irr,0}$ after all, and that θ (or HT schedule in general) is far more important. The reason for our previous results that suggested higher $\varepsilon_{irr,0}$ for Ti-doped conductors resides in the fact that SIC is shifted to lower values of θ for these wires as compared to Ta-alloyed wires, and that θ in our previous studies (640 °C) was favorable to Ti-doped wires⁵.

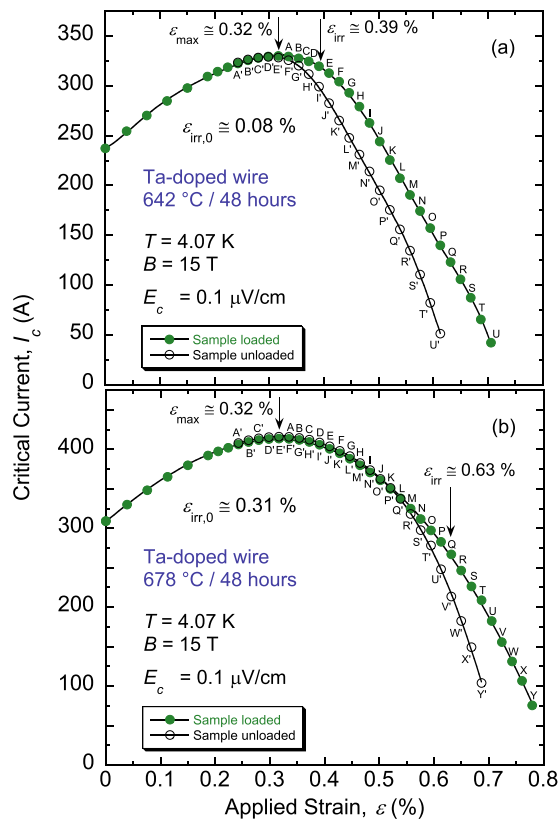


Figure 3. Examples of $I_c(\varepsilon)$ at 4.07 K and 15 T for samples of an RRP Ta-doped Nb_3Sn wire (billet 13711-2), heat-treated for 48 hours at (a) 642 °C and (b) 678 °C. The intrinsic irreversible strain limit $\varepsilon_{\text{irr},0}$ ($=\varepsilon_{\text{irr}} - \varepsilon_{\text{max}}$) is significantly improved for the sample heat-treated at 678 °C in comparison to that reacted at 642 °C (0.31% vs. 0.08%, respectively), indicating a strong dependence of $\varepsilon_{\text{irr},0}$ on the heat-treatment temperature θ . The sample was loaded and partially unloaded (by constant axial-strain steps of about 0.09%) to obtain the “loaded” and “unloaded” $I_c(\varepsilon)$ curves, represented by solid and empty symbols, respectively. As in Fig. 1, corresponding loaded and unloaded points are labelled by unprimed and primed letters, respectively.

In practical terms, the HT schedule for the LHC magnets must be chosen very carefully to balance not only the needs for high RRR and high I_c , but the need for high $\varepsilon_{\text{irr},0}$ too, to ensure mechanical integrity of the conductors. Recently, a requirement for $\varepsilon_{\text{irr},0} > 0.25\%$ was added to the strand design criteria for the fabrication of the LHC quadrupole magnets (referred to as MQXF)¹⁷. Steepness of SIC implies that special attention must be paid to the homogeneity and precision of temperature in the furnaces to be used for heat-treating these large, several meters long, and massive magnets. This is particularly true if the targeted value of θ is around the SIC tip (which happens to be at 640 °C for the Ti-doped wire studied here). If θ chosen is at, or close to, the precipitous drop of SIC, temperature gradient across the magnet during heat treatment and temperature imprecision in the furnace may yield regions in the magnet with small values of $\varepsilon_{\text{irr},0}$. Such weak regions may dictate the magnet performance. The name *strain irreversibility cliff* was chosen to convey a cautionary message to magnet developers that the risk of magnet failure is sufficiently high to warrant precautionary measures.

We note that another report showed a dependence of $\varepsilon_{\text{irr},0}$ on θ ¹⁸. Though the results therein were limited between 610 and 650 °C and resemblance to the shape of SIC is not evident, the general trend seems consistent.

Implications on heat-treatment optimization. Figure 4(b) represents $I_{c-\text{max}}(\theta)$, the value of I_c at the applied strain ε_{max} that compensates for the sample’s pre-compressive strain (note that the sample is soldered to a thick Cu-Be Walters spring; see explanations in the section “Methods” below). $I_{c-\text{max}}$ is used here to monitor the effect of θ on I_c at this reference strain around which the I_c dependence on strain is small^{11,19}. $I_{c-\text{max}}$ depends strongly on θ and reaches a maximum at approximately 680 °C for both wires. The increase of $I_{c-\text{max}}$ with θ (for $\theta < 680$ °C) is because more Nb_3Sn material is formed, resulting in an increase of the superconductor cross-sectional area. It also originates from the composition of Nb_3Sn that gradually becomes more homogeneous and closer to stoichiometry, which improves the superconductor’s effective upper critical-field and critical temperature^{8,20–22}.

Microstructural studies, conducted by use of a field-emission scanning electron microscopy (FESEM) on a selection of samples, showed effectively an increase of the A15 area for the Ta-doped samples reacted at 678 °C as compared to 642 °C (Table 1). The increase in area is 8.6%, so it counts only partially for the increase of I_c that is 25.3% between these two HTs for this Ta-doped wire. Thus, most of the I_c increase is related to the A15 reaction producing a composition that is more homogeneous and closer to stoichiometry, as more Sn is consumed

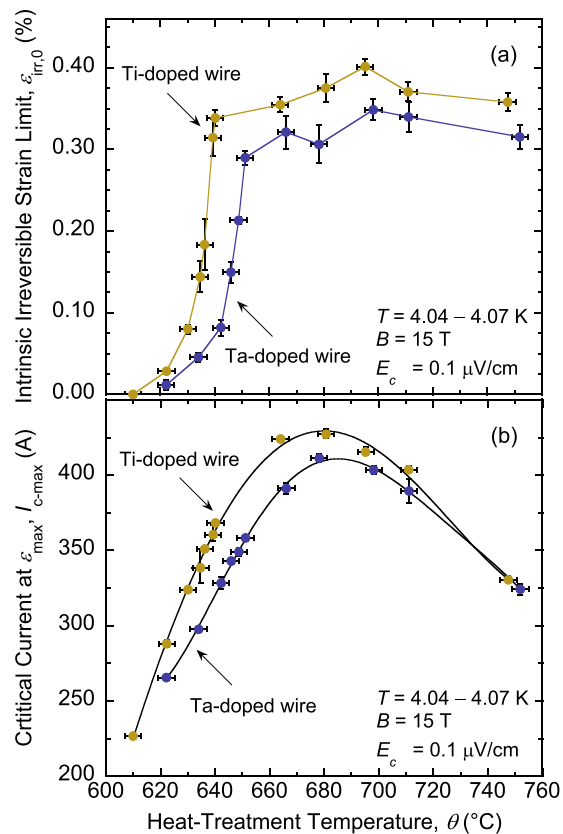


Figure 4. (a) Precipitous change of $\epsilon_{irr,0}(\theta)$ found in RRP Nb₃Sn wires, either doped with Ti (billet 11976-1) or Ta (billet 13711-2). We named this behavior the *strain irreversibility cliff*. It is shifted to lower temperatures by 10 to 12°C for the Ti-doped wire as compared to that of the Ta-doped wire. (b) $I_{c-max}(\theta)$ dependence for the same RRP Nb₃Sn wires, showing that I_{c-max} is highest at approximately 680°C for both wires. The non-Cu areas for RRP billets 11976-1 and 13711-2 were 48.9% and 46.5% of the wires cross-sections, respectively. The error bars shown for $\epsilon_{irr,0}$ and I_{c-max} values correspond to twice the standard error of their respective mean, $2\frac{s}{\sqrt{n}}$, where s is the standard deviation and n is the number of segments used to calculate the mean. The error bars for θ values correspond to $\pm 3^\circ\text{C}$.

HT temperature θ /duration	Sub-elements equivalent diameter (μm)	Sub-elements A15 area (%)	Sub-elements unreacted-barrier area (%)	Unreacted-barrier thickness (μm)	Maximum barrier thickness (μm)	Minimum barrier thickness (μm)	Sub-elements with reacted-through barrier (%)	Sub-elements with unreacted-barrier-thickness $< 0.5 \mu\text{m}$ (%)
642°C/48h	51.1	57.1	9.5	1.22 ± 0.35	3.1	0.06	0.0	0.89
678°C/48h	52.5	62.0	5.8	0.70 ± 0.36	2.5	0.00	4.9	32.7

Table 1. Analysis of sub-elements' A15 area and unreacted Nb barrier for the RRP Ta-doped Nb₃Sn wire (billet 13711-2).

in the reaction as a result of increasing θ . The spatial variation of elemental compositions of Nb, Ta, Sn, and Cu, mapped by use of field-emission scanning-electron microscopy, energy-dispersive spectroscopy (FESEM-EDS) and depicted in Fig. 5, shows more prominent Sn-rich rings around the original Nb filaments in the samples reacted at 642°C as compared to 678°C. Hence, samples reacted at 678°C have a more homogeneous Sn spatial distribution that should lead to a more homogeneous Nb₃Sn composition across the A15 layer (see²¹ for more extensive FESEM-EDS mapping). Whether the composition homogenization and stoichiometry are part of the mechanisms that give rise to SIC (and to the reduction of I_c irreversible-degradation rate as in Fig. 2) remains an open question. We will examine the SIC mechanisms in future reports.

The improvements of A15 area and quality are countered by a progressive growth of Nb₃Sn grains that reduces the density of grain boundaries—the main pinning centers of magnetic flux lines in Nb₃Sn material—and weakens the bulk pinning strength as a result^{23–25}. For $\theta > 680^\circ\text{C}$, even as A15 area and quality most likely continue to improve with increasing θ , weakening of flux pinning becomes more dominant than these and causes the decline of I_{c-max} (Fig. 4(b)). We do not expect Nb₃Sn grain growth to be a contributing factor in the occurrence of SIC,

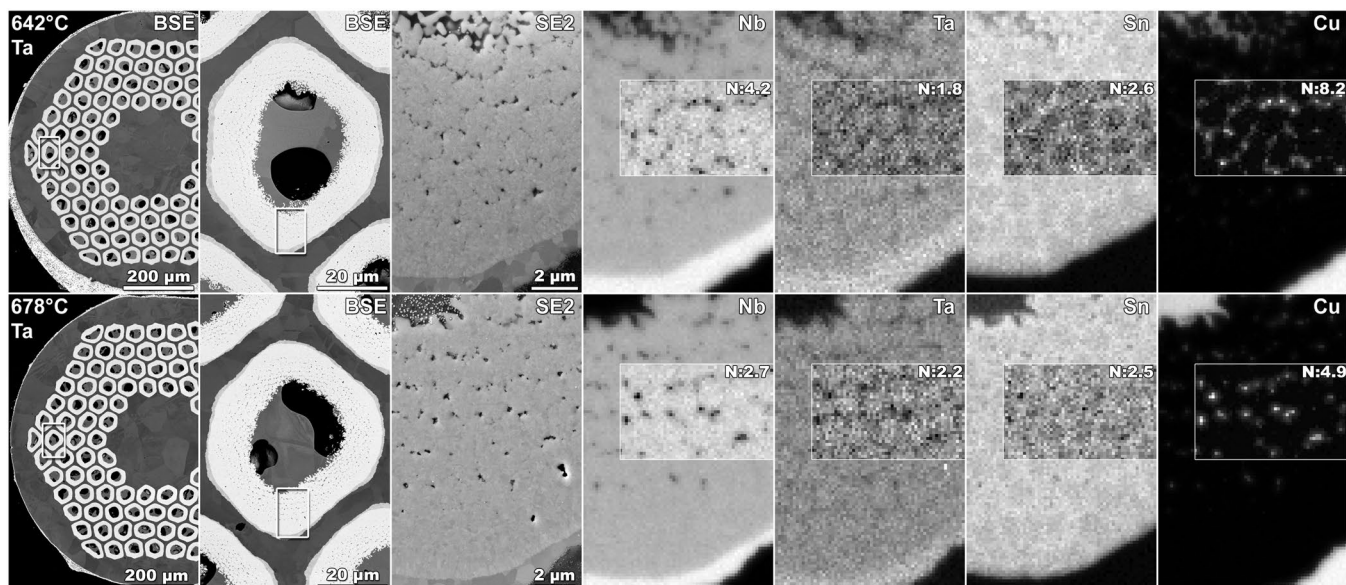


Figure 5. Field emission scanning electron microscopy (FESEM) images of RRP Nb₃Sn Ta-doped wire (billet 13711–2) cross-sections, for samples heat treated for 48 hours at 642 °C (top row) and 678 °C (bottom row), respectively. (For reference, examples of $I_c(\varepsilon)$ data for these samples or similar are depicted in Fig. 3). The three left columns show atomic-number sensitive back-scattered electron (BSE) images, where the dark dots in the third column represent voids and remaining Cu islands within the portion selected of a sub-element pack highlighted in the first two columns. The subsequent four columns at the right are energy dispersive spectroscopy (EDS) qualitative compositional maps for Nb, Ta, Sn, and Cu within the same highlighted areas, where the brightest spots are regions with the highest atomic composition of the mapped element. Spatial distribution of Sn is clearly more inhomogeneous for 642 °C in comparison to 678 °C. To reveal minor variations in composition within the filament pack, the map contrast in the outlined boxes has been normalized to maximize contrast in the insets for each element. The values used for the contrast normalization factor N in each case are shown in the corresponding inset. N is defined as the ratio of the expanded intensity range and the initial intensity range.

nevertheless. The guidelines that emerge from Fig. 4(a,b) is that θ should be higher than that corresponding to the SIC tip and as close to 680 °C as possible to ensure adequate mechanical and transport properties of the wires. However, RRR specifications impose additional constraints that will restrict the range of θ that can fulfill all these requirements at once, as discussed below.

The finding of the SIC profoundly changed the common perception that $\varepsilon_{irr,0}$ is essentially inherent to the wire once fabricated, and cannot be manipulated as easily as the other strand properties such as J_c and RRR through HT. Optimization of $\varepsilon_{irr,0}$, now clearly possible, faces the same dilemma as optimizing J_c without driving RRR too low. An ideal HT for the Ta-doped wire, for example, would be around 678 °C, which maximizes J_c and positions $\varepsilon_{irr,0}$ comfortably at the top of SIC (Fig. 4). However, the Nb barrier distributed around each sub-element—to prevent Sn from poisoning Cu matrix during HTs so as to preserve high RRR—becomes very thin at 678 °C. It has an average thickness of 0.7 μm, with a third of the sub-elements having a barrier less than 0.5 μm thick (Table 1). More importantly, it is breached at some locations. As shown in Table 1, 4.9% of sub-elements have reacted-through barriers. From the correlation between the percent react-through barriers and RRR proposed in²¹, we project an RRR just slightly above 50 at this HT, far below the minimum value of 150 required (for undeformed strands) for the LHC high-luminosity upgrade. So, θ must be reduced below 678 °C to meet the RRR requirement. Yet, it must not be lower than 651 °C, the temperature of the SIC tip for this wire, so that $\varepsilon_{irr,0}$ is not compromised either. This simple example illustrates how narrow is the choice of θ that would fulfill both RRR and $\varepsilon_{irr,0}$ requirements, at least for the wires studied here. It may be possible to lower θ below 651 °C and increase the dwell time—highly recommended for achieving more uniform HT of massive magnets—to reach HT conditions that preserve high $\varepsilon_{irr,0}$. We will address these questions in detail elsewhere. Analysis of the complete $I_c(\varepsilon)$ irreversible degradation dataset is also beyond the scope of this report.

The message from the finding of SIC is that the trade-off between RRR and J_c must encompass the wire's strain properties too, given that a compromise on J_c in order to obtain high RRR could depress $\varepsilon_{irr,0}$ severely and dangerously. This trade-off must be scrutinized very closely for the LHC high-luminosity upgrade. We do not know if Nb₃Sn conductors made for the International Thermonuclear Experimental Reactor (ITER), particularly wires made by the internal-tin process, exhibit the SIC behavior¹¹. We recommend that it be checked, especially because ITER Nb₃Sn magnets are even more massive and a tight control of their temperature during heat treatment could be very challenging.

Methods

Walters spring apparatus. Each RRP Nb₃Sn sample had a length of approximately 2.5 meters. It was wound on a grooved stainless-steel mandrel and heat-treated at a given final temperature. The helical-shaped sample was then carefully transferred onto a Walters' spring device for applying strain to the sample *in-situ*^{13,14}. The spring is made of a Cu-Be alloy and its turns have the same pitch as the groove of the reaction mandrel. It has a wide elastic strain range from -1% to +1%^{14,15}, and can be strained by twisting its top end with respect to the bottom end. Prior to using it for sample measurements, strain gages were mounted on the outer surface of the spring turns for the purpose of calibrating applied strain as a function of angular displacement of the spring ends¹⁴. Each Nb₃Sn sample was soldered to the spring along its full length.

Upon cooling the apparatus to helium temperature, Cu-Be spring puts an additional pre-compression onto Nb₃Sn sample because Cu-Be has a higher thermal expansion coefficient than Nb₃Sn wires and the thick spring dominates the thermal compression of the assembly¹¹. Consequently, the measured values of ϵ_{\max} and the irreversible strain limit ϵ_{irr} (examples shown in Figs 1 and 3) are artificially high. However, the values of $\epsilon_{\text{irr},0}$ ($=\epsilon_{\text{irr}} - \epsilon_{\max}$) are not affected by the spring material's differential thermal contraction and, therefore, are correct^{11,19}. For reference, the actual values of ϵ_{\max} for RRP wires should be rather small, given the high Nb fraction in RRP wires as compared to other Nb₃Sn conductors such as ITER wires for example²⁶.

Microscopy description. Electron microscopy on metallographically polished wire cross-sections was performed using a Zeiss 1540 EsB field emission scanning electron microscope (FESEM). Energy dispersive spectroscopy (EDS) was performed in the FESEM using an EDAX Apollo XP solid state x-ray detector at an accelerating voltage of 15 kV.

References

- Rossi, L. Superconductivity: its role, its success and its setbacks in the Large Hadron Collider of CERN. *Supercond. Sci. Technol.* **23**, 034001 (2010).
- Bottura, L. & Godeke, A. Superconducting materials and conductors: fabrication and limiting parameters. *Rev. Accel. Sci. Technol.* **5**, 25–50 (2012).
- Ferracin, P. *et al.* Development of MQXF: the Nb₃Sn low- β quadrupole for the HiLumi LHC. *IEEE Trans. Appl. Supercond.* **26**, 4000207 (2016).
- Parrell, J. A. *et al.* Internal tin Nb₃Sn conductors engineered for fusion and particle accelerator applications. *IEEE Trans. Appl. Supercond.* **19**, 2573–2579 (2009).
- Cheggour, N. *et al.* Influence of Ti and Ta doping on the irreversible strain limit of ternary Nb₃Sn superconducting wires made by the restacked-rod process. *Supercond. Sci. Technol.* **23**, 052002 (2010).
- Sheuerlein, C. *et al.* Texture in state-of-the-art Nb₃Sn multifilamentary superconducting wires. *Supercond. Sci. Technol.* **27**, 025013 (2014).
- Peng, X. *et al.* Strain and magnetization properties of high subelement count tube-type Nb₃Sn strands. *IEEE Trans. Appl. Supercond.* **21**, 2559–2562 (2011).
- Cooley, L. D., Ghosh, A. K., Dietderich, D. R. & Pong, I. Conductor specification and validation of high-luminosity LHC quadrupole magnets. *IEEE Trans. Appl. Supercond.* **27**, 6000505 (2017).
- Ghosh, A. K. Effect of copper resistivity and filament size on the self-field instability of high- J_c Nb₃Sn strands. *IEEE Trans. Appl. Supercond.* **23**, 7100407 (2013).
- Bordini, B., Bottura, L., Oberli, L., Rossi, L. & Takala, E. Impact of the residual resistivity ratio on the stability of Nb₃Sn magnets. *IEEE Trans. Appl. Supercond.* **22**, 4705804 (2012).
- Cheggour, N. *et al.* Influence of the heat-treatment conditions, microchemistry, and microstructure on the irreversible strain limit of a selection of Ti-doped internal-tin Nb₃Sn ITER wires. *Supercond. Sci. Technol.* **27**, 105004 (2014).
- Goodrich, L. F. *et al.* Method for determining the irreversible strain limit of Nb₃Sn wires. *Supercond. Sci. Technol.* **24**, 075022 (2011).
- Walters, C. R., Davidson, I. M. & Tuck, G. E. Long sample high sensitivity critical current measurements under strain. *Cryogenics* **26**, 406–412 (1986).
- Cheggour, N. & Hampshire, D. P. A probe for investigating the effects of temperature, strain, and magnetic field on transport critical currents in superconducting wires and tapes. *Rev. Sci. Instrum.* **71**, 4521–4530 (2000).
- Goodrich, L. F., Cheggour, N., Stauffer, T. C., Filla, B. J. & Lu, X. F. Kiloampere, variable-temperature, critical-current measurements of high-field superconductors. *J. Res. NIST* **118**, 301–352 (2013).
- Joint Committee for Guides in Metrology 2008a. *Evaluation of measurement data — guide to the expression of uncertainty in measurement*. BIPM, IEC, IFCC, ILAC, ISO, IUPAC, IUPAP, and OIML, JCGM 100:2008, GUM 1995 with minor corrections, https://www.bipm.org/utls/common/documents/jcgm/JCGM_100_2008_E.pdf.
- Anderssen, E. *et al.* *Design criteria for MQXFA superconducting elements*. US HL-LHC Accelerator Upgrade Project, <https://indico.fnal.gov/event/16858/contribution/1/material/0/0.pdf>.
- Lu, J. *et al.* Characterization of high J_c Nb₃Sn strands for the series-connected hybrid magnet. *IEEE Trans. Appl. Supercond.* **19**, 2615–2618 (2009).
- Cheggour, N. *et al.* Strain and magnetic-field characterization of a bronze-route Nb₃Sn ITER wire: benchmarking of strain measurement facilities at NIST and University of Twente. *IEEE Trans. Appl. Supercond.* **22**, 4805104 (2012).
- Tarantini, C., Sung, Z.-H., Lee, P. J., Ghosh, A. K. & Larbalestier, D. C. Significant enhancement of compositional and superconducting homogeneity in Ti rather than Ta-doped Nb₃Sn. *Appl. Phys. Lett.* **108**, 042603 (2016).
- Tarantini, C., Lee, P. J., Craig, N., Ghosh, A. & Larbalestier, D. C. Examination of the trade-off between intrinsic and extrinsic properties in the optimization of a modern internal tin Nb₃Sn conductor. *Supercond. Sci. Technol.* **27**, 065013 (2014).
- Ghosh, A. K., Sperry, E. A., D'Ambra, J. & Cooley, L. D. Systematic changes of the Nb-Sn reaction with time, temperature, and alloying in restacked-rod-process (RRP) Nb₃Sn strands. *IEEE Trans. Appl. Supercond.* **19**, 2580–2583 (2009).
- Scanlan, R. M., Fietz, W. A. & Koch, E. F. Flux pinning centers in superconducting Nb₃Sn. *J. Appl. Phys.* **46**, 2244–2249 (1975).
- Osamura, K., Ochiai, S., Kondo, S., Namatame, M. & Nosaki, M. Influence of third elements on growth of Nb₃Sn compounds and on global pinning force. *J. Mater. Sci.* **21**, 1509–1516 (1986).
- Osamura, K. & Ochiai, S. Flux pinning in A15 superconductors. *Jpn. J. Appl. Phys.* **26**, 1519–1520 (1987).
- Ekin, J. *et al.* Compressive pre-strain in high-niobium-fraction Nb₃Sn superconductors. *IEEE Trans. Appl. Supercond.* **15**, 3560–3563 (2005).

Acknowledgements

This work was supported by the U.S. Department of Energy, Office of High Energy Physics, Grants DE-SC0010690, DE-SC0017657, FG02-07ER41451, and DE-SC0012083. A portion of this work was performed at the National High Magnetic Field Laboratory, supported by the National Science Foundation Cooperative Agreement No. DMR-1157490 and the State of Florida. Nb₃Sn RRP wires were provided by the U.S. Conductor Development Program (CDP), managed by D. Dieterich at the Lawrence Berkeley National Laboratory (LBNL) and supported by DOE contract number DE-AC02-05CH11231 and LBNL. RRP is a registered trademark of Oxford Instruments, Superconducting Technology. Certain commercial materials are specified in order to adequately describe the experiment; endorsement by NIST is not implied. N. Cheggour is a NIST Associate. Contribution of NIST, an agency of the U.S. government, not subjected to copyright.

Author Contributions

N.C. designed the study, performed the electromechanical measurements, analyzed the data, and prepared the manuscript. T.C.S. mounted the samples on the Walters' strain device and apparatus. W.S. prepared the samples and conducted 17 heat-treatment cycles. P.J.L. performed FESEM studies and FESEM-EDS mapping, and analyzed the sub-elements' A15 area and unreacted Nb barrier. J.D.S. developed the software for analyzing the irreversible strain limit and analyzed the underlying critical-current vs. strain data to extract the irreversible-strain-limit values. L.F.G. developed the software for acquiring transport data and for analyzing the irreversible strain limit. A.K.G. selected the wires to be studied and conducted 6 heat-treatment cycles. N.C., L.F.G. and T.C.S. designed and commissioned the Walters' strain apparatus. All authors discussed the results and commented on the manuscript.

Additional Information

Competing Interests: The authors declare no competing interests.

Publisher's note: Springer Nature remains neutral with regard to jurisdictional claims in published maps and institutional affiliations.



Open Access This article is licensed under a Creative Commons Attribution 4.0 International License, which permits use, sharing, adaptation, distribution and reproduction in any medium or format, as long as you give appropriate credit to the original author(s) and the source, provide a link to the Creative Commons license, and indicate if changes were made. The images or other third party material in this article are included in the article's Creative Commons license, unless indicated otherwise in a credit line to the material. If material is not included in the article's Creative Commons license and your intended use is not permitted by statutory regulation or exceeds the permitted use, you will need to obtain permission directly from the copyright holder. To view a copy of this license, visit <http://creativecommons.org/licenses/by/4.0/>.

© The Author(s) 2018